Evapotranspiration Prediction and Irrigation Scenario Analysis Based on Physics-XGBoost

Guoqing Zhang, Miao Huang, Lili Tao, and Shuping Zhang

***Abstract*—Accurate prediction of transpiration rate is crucial for precision irrigation and improved water use efficiency in greenhouses. This paper proposes a "Physics + XGBoost + Shapley additive explanation (SHAP)" framework. A physical indicator, E_{phys} = Cond × VpdL, is constructed using stomatal conductance (Cond) and leaf-air vapor pressure deficit based on leaf temperature (VpdL) to establish a linear physical baseline. Subsequently, an XGBoost residual correction model is built using the residual between observed transpiration rate and the predicted physical value as the learning objective, thus forming the Physics + XGBoost transpiration rate prediction framework. Results show that the coefficient of determination on the test set is approximately 0.9975, and the root mean square error is approximately 0.0583. SHAP analysis indicates that E_{phys}, Cond, and VpdL are the dominant factors driving residual correction. Furthermore, this paper predicts the canopy daily evapotranspiration at the leaf scale to construct an irrigation scenario, providing a generalizable technical path for water management and physical-data fusion modeling of greenhouse crops.**

***Index Terms*—Evapotranspiration prediction, physics-informed machine learning, XGBoost, irrigation scheduling optimization, scenario analysis**

I. Introduction

AGAINST the backdrop of global climate change and increasing water scarcity, predicting plant transpiration rate has become a focus of attention in the agricultural field. Photosynthetic rate, stomatal conductance, and transpiration rate at the leaf scale are three core parameters of carbon-water exchange in plants. In drip-irrigated greenhouse production, crop evapotranspiration is typically dominated by plant transpiration, whereas soil evaporation is comparatively smaller under covered/mulched conditions [1]. Transpiration rate plays a key coordinating role among them, directly affecting the plant's water consumption intensity, drought tolerance, and photosynthetic productivity [2, 3].

Theoretical studies have shown that intrinsic water use efficiency (iWUE) can effectively summarize the trade-off between leaf carbon assimilation and water loss, and has been widely used as a quantitative indicator across different species and environmental gradients [4–6]. Transpiration not only reflects water loss, but also plays an important role in leaf temperature regulation, physiological metabolism, and optimal stomatal behavior [7, 8]. Evaporative cooling associated with transpiration can substantially regulate leaf temperature [9], and the transpiration stream supports long-distance transport of water and dissolved nutrients through the soil-plant-atmosphere continuum [10, 11]. However, the quantitative application of indicators that more directly reflect the cost of transpiration, such as transpiration cost per unit of photosynthetic yield, at the leaf scale remains limited, which to some extent restricts the in-depth analysis of the carbon-water synergistic optimization mechanism from a data perspective.

The classic photosynthesis-stomatal-transpiration coupling framework provides a foundation for understanding leaf-scale carbon-water coupling by jointly solving the Farquhar model, the Ball-Berry model, and the energy balance equation [12, 13]. These models generally implicitly contain the first-order physical relationship $E \approx g_s \times \mathrm{VPD}$, that is, transpiration is mainly determined by stomatal conductance (g_s) and leaf-air vapor pressure deficit (VPD), which is also supported by VPD gradient experiments and review work [14]. However, in specific applications, they often face problems such as numerous parameters, high acquisition costs, insufficient expression of some nonlinear processes, and limited portability in cross-species and cross-environment scenarios [8, 15]. Moreover, routine greenhouse climate-control operations (e.g., ventilation, shading, heating, and fogging/humidification) can rapidly reshape radiation and humidity, thereby shifting VPD and inducing strong within-day and day-to-day variability in transpiration [16, 17]. Under such variability, fixed-timer or experience-based irrigation may fail to track actual crop demand, leading to transient water deficits on high-demand days or unnecessary drainage/leaching on low-demand days and reduced water-use efficiency [18].

On the other hand, although gas exchange systems, such as LI-6400, have been successfully used to measure transpiration and photosynthesis in crops and natural vegetation, they still lack a systematic characterization of nonlinear transpiration responses driven by multiple variables [19, 20]. Most studies still focus on validating specific mechanistic models or

Manuscript received: 27 January 2026; revised: 2 March 2026; accepted: 4 March 2026. *(Corresponding author: Shuping Zhang.)*

Citation: G. Zhang, M. Huang, L. Tao, and S. Zhang, Evapotranspiration prediction and irrigation scenario analysis based on physics-XGBoost, *Int. J. Intell. Control Syst.*, 2026, 31(1), 16–28.

Guoqing Zhang, Miao Huang, and Lili Tao are with School of Intelligent Manufacturing and Control Engineering, Shanghai Polytechnic University, Shanghai 201209, China (e-mail: SSPU_1281960805@163.com; huangmiao@sspu.edu.cn; lltao@sspu.edu.cn).

Shuping Zhang is with School of Intelligent Medicine and Health Engineering, Shanghai Polytechnic University, Shanghai 201209, China (e-mail: spzhang@sspu.edu.cn).

Digital Object Identifier 10.62678/IJICS202603.10291

comparing treatment differences, lacking a systematic characterization of high-dimensional nonlinear transpiration responses driven by multiple variables, especially lacking quantitative analysis that integrates g_s, VPD, and iWUE indices into the same framework.

In recent years, machine learning has provided new possibilities for modeling evapotranspiration and crop water consumption. Boosting tree models, such as XGBoost, have shown high accuracy and strong robustness in evapotranspiration prediction, leaf functional trait estimation, and crop water consumption simulation [21–24]. On a larger scale, hybrid models have effectively improved the stability of predictions under extreme conditions and across regions by combining physical mechanisms with data-driven methods [25–27]. However, existing studies mostly focus on the canopy or regional scale, and pay little attention to transpiration modeling at the leaf scale, especially the "physical prior + interpretable machine learning" framework. Most machine learning studies do not explicitly include physical driving variables related to transpiration such as g_s and vapor pressure deficit based on leaf temperature (VpdL), and lack process explanation based on Shapley additive explanation (SHAP) [28]. The quantitative connection between model results and clean production goals such as water conservation, energy conservation, and emission reduction is still not close enough. XGBoost was employed for residual correction because the transpiration response involves strong nonlinearities and interactions between physiological and environmental variables, and gradient boosting trees effectively capture these characteristics on tabular datasets. More importantly, learning the residuals ($E - \hat{E}_{\text{phys}}$, where $\hat{E}_{\text{phys}}$ indicates the physical baseline) constrains the model to missing nonlinear components beyond the first-order physical processes, thereby improving model robustness and reducing the risk of learning spurious correlations. This physical process-based residual formulation also aids in interpretation, as SHAP can reveal how specific factors alter the physical baseline under different conditions. Therefore, it is necessary to construct a transpiration modeling system at the leaf scale that has physical consistency, high prediction accuracy, and strong interpretability.

To address the above shortcomings, this paper constructs a unified dataset that includes transpiration rate, photosynthetic rate, stomatal conductance, leaf-air vapor pressure difference, and environmental variables, and derives key physical-physiological indicators: E_{phys} is used to display the stomatal-transpiration mechanism at the feature level; iWUE is used to evaluate plant adaptation strategies and long-term water use patterns [29]; and cost of transpiration per unit photosynthetic rate (CTE) is convenient for analyzing water use efficiency and stomatal optimization hypothesis from the perspective of transpiration cost [30].

Based on the above problems, this paper focuses on the chain of "physical consistency-high accuracy-interpretability-decision-making capability", with the following main innovations. First, for transpiration rate prediction, a calibrable physical baseline is constructed with E_{phys} = Cond × VpdL as the core, and a lifting tree is used to perform nonlinear correction on the residuals, thereby improving the fitting ability under complex conditions while maintaining consistency in physical magnitude and trend. Second, SHAP is used to achieve interpretability analysis, revealing the nonlinear correction mechanism of transpiration from the contributions of features such as VpdL, Cond, and E_{phys}, making up for the problem of the "black box" difficulty in interpretation in traditional machine learning. Third, the leaf-scale transpiration prediction results are converted to units and combined with leaf area index (LAI) to construct a comparison between on-demand irrigation and empirical irrigation scenarios, realizing the quantitative transfer from leaf physiological processes to irrigation water parameters, and providing a decision-making basis for water management of facility crops.

Therefore, transpiration prediction serves as a key variable linking greenhouse environmental regulation to crop water demand and ultimately to irrigation decision-making.

A. Experimental Materials

a. Data Source

The data used in this study came from a public dataset [20]. This dataset was based on the actual measurement of leaf gas exchange of greenhouse-grown tomatoes. A total of 16 observation days were selected from November 2019 to January 2020, with each day lasting about 6 h, and the photosynthetic rate, transpiration rate, stomatal conductance, and corresponding environmental variables of the leaves were recorded.

b. Physiological Indicators

The original data table contains the main blade gas exchange variables and environmental factors output by the LI-6400XT. The variables that are the focus of this paper are shown in Table 1.

Table 1 Environmental factor data.

No.	Symbol	Explanation
1	Trmmol	Transpiration rate
2	Photo	Photosynthetic rate
3	Cond	Conductance to H_2O
⋮	⋮	⋮
19	C_i/C_a	Intercellular CO_2/Ambient CO_2
20	vp_kPa	Vapor pressure chamber air

Building upon this, to explicitly incorporate the classical stomatal-transpiration mechanism and the concept of water use efficiency into the model structure, facilitating the mechanistic interpretation of machine learning results in subsequent analyses, the following derived indices with clear physical and physiological meanings were constructed:

1. Prior quantity of physical transpiration

$$E_{\text{phys}} \approx \text{Cond} \times \text{VpdL} \tag{1}$$

Leaf transpiration is primarily a diffusion flux, which can be approximated by a first-order relation: $E \approx g_s \times$ VpdL in the classical stomatal model. It is considered a "first-order physics prediction" of leaf transpiration based on stomatal conductance and vapor pressure difference, neglecting energy balance details.

In Eq. (1), Cond represents the effective stomatal channel conductance and VpdL represents the vapor pressure driving force. Other environmental factors mainly exert their influence by adjusting Cond and/or the blade-air VPD, while the remaining nonlinearities are handled by a residual correction model.

2. Intrinsic water use efficiency

$$\mathrm{iWUE} = \frac{\mathrm{Photo}}{\mathrm{Cond}} \tag{2}$$

The net photosynthetic gain per unit stomatal conductance reflects the trade-off between photosynthetic carbon gain and water loss.

3. CO_2 ratio inside and outside the leaf

$$\frac{C_\mathrm{i}}{C_\mathrm{a}} = \frac{C_\mathrm{i}}{C_\mathrm{ref}} \tag{3}$$

C_ref is measured by the reference channel CO_2 (such as CO2R in the dataset used in this paper), which is used to characterize the degree of stomatal limitation and is closely related to photosynthetic regulation and WUE.

4. Cost per unit of photosynthetic transpiration

$$\mathrm{CTE} = \frac{\mathrm{Trmmol}}{\mathrm{Photo}} \tag{4}$$

Representing the transpiration "cost" required to produce a unit net photosynthetic rate helps to discuss WUE and stomatal optimization theory from the perspective of "transpiration cost".

c. Data Processing

All original files are read and merged into a single data table. Date and time information are standardized to generate date and timestamp variables, which are then sorted by date and time to construct a time-series consistent dataset.

Missing value handling: Records containing missing values are deleted to ensure the integrity of subsequent derived indicators and modeling.

Physical range constraints and outlier removal: Reasonable thresholds are set for key variables to remove observations that are obviously unreasonable or suspected of measurement errors. This aims to eliminate instrument noise and extreme observations while preserving normal physiological fluctuations as much as possible.

(1) Photosynthetic rate is limited to $-5 < A < 50$ μmol $CO_2 \cdot m^{-2} \cdot s^{-1}$ to remove nighttime noise and extreme outliers;

(2) Stomatal conductance is limited to $0 < g_s < 1.2$ mol $H_2O \cdot m^{-2} \cdot s^{-1}$, and transpiration rate is limited to $0 < E < 25$ mmol $H_2O \cdot m^{-2} \cdot s^{-1}$;

(3) Leaf-aerosol vapor pressure difference is limited to $0 \leqslant \mathrm{VpdL} < 5$ kPa.

Derived indicator calculation and variable reconstruction: After handling missing and outlier values, derived indicators such as E_phys, iWUE, CTE, and $C_\mathrm{i}/C_\mathrm{a}$ are calculated for each record, and the results are added as new columns for subsequent modeling and interpretation.

Dataset partitioning: To avoid time series leakage, the dataset is partitioned by observation date. After sorting the data from earliest to latest, 70% of the observation days are allocated to the training set, 15% to the validation set, and 15% to the test set.

B. Modeling Methods

This paper adopts a technical approach of "Physics + XGBoost residual correction + SHAP interpretability + scenario construction". First, a physical transpiration baseline is constructed based on E_phys to characterize the traditional $E \approx g_s \times \mathrm{VPD}$ mechanism. Then, an XGBoost model and a fused residual model are constructed to compare the performance differences of multiple models. SHAP is used to analyze the influence of features such as E_phys, VpdL, and Photo on transpiration prediction correction. Finally, leaf-scale prediction is combined with canopy-scale evapotranspiration and irrigation scenario analysis. The technical roadmap for transpiration rate modeling is shown in Fig. 1.

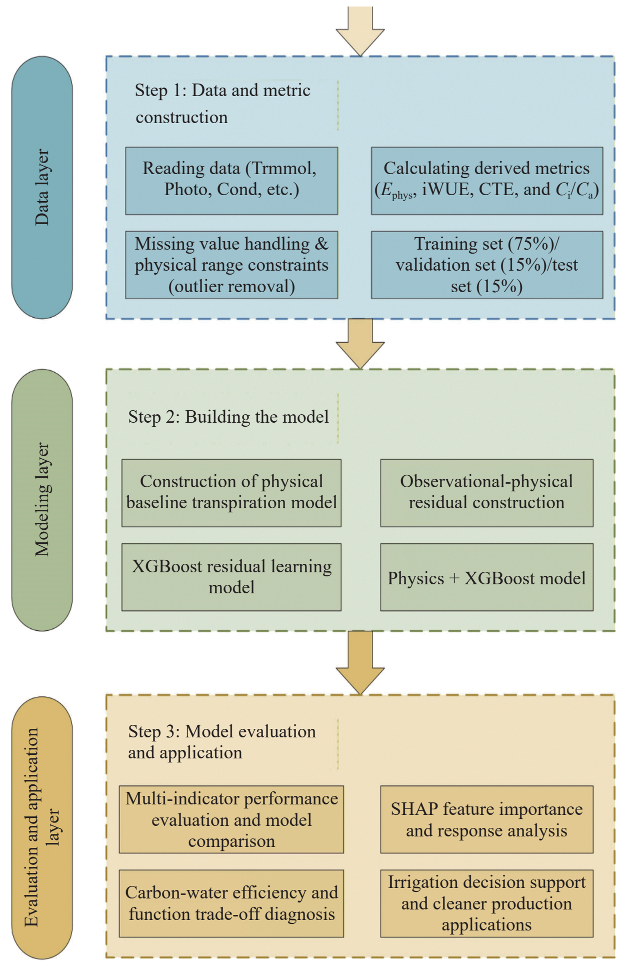

Fig. 1 Technology roadmap.

a. Physical Baseline Model

By incorporating the classic stomatal-transpiration mechanism into the modeling framework, a linear regression model based solely on the physical prior quantity E_phys is constructed as the physical baseline for transpiration prediction. The physical baseline model is

$$E_i = aE_{\mathrm{phys},i} + b + \varepsilon_i \tag{5}$$

where E_i is the transpiration rate, i is the observed sample, $E_{\mathrm{phys},i}$ is the physical estimate of the transpiration rate E_i, a and b are estimated on the training set using ordinary least squares, and ε_i is the residual term.

This model embodies the linear relationship $E \approx g_s \times \text{VpdL}$ and can be viewed as a first-order approximation of the leaf transpiration process. The trained linear model is used to predict the physical baseline value E^*_{phys} on the training, validation, and test sets, respectively.

b. XGBoost Data-Driven Model

Beyond the physical baseline, a data-driven model is constructed using the gradient boosting tree algorithm XGBoost, with leaf transpiration rate E as the output and physiological and environmental variables as the input feature vector.

The XGBoost model is $f_\theta(\cdot)$, and the data-driven model is

$$\hat{E}_{\text{XGB},i} = f_\theta(x_i) \tag{6}$$

where θ represents the model parameter learned on the training set using the gradient boosting algorithm, and x_i represents the input features.

c. Physics + XGBoost Fusion Residual Model

To balance physical consistency and prediction accuracy, a fusion residual model is constructed between the physical baseline and XGBoost. The physical baseline is used to obtain the physical prediction value E^*_{phys} for each sample. Then, the residual is used as the new learning objective, and XGBoost is used to fit the remaining nonlinear component. Let the residual be

$$r_i = E_i - E^*_{\text{phys},i} \tag{7}$$

The residual model can then be expressed as

$$\hat{r} = g\phi(x_i) \tag{8}$$

where $g\phi(\cdot)$ is an XGBoost regression model with x_i as input and residual r_i as output, and ϕ is its parameter. The final fusion prediction is

$$\hat{E}_{\text{fusion},i} = E^*_{\text{phys},i} + \hat{r}_i \tag{9}$$

This "physical baseline + residual learning" approach treats the physical model as a first-order approximation of evaporation, and then XGBoost corrects the remaining nonlinearities and interaction effects. This approach can maintain the prediction results in terms of magnitude and trend in accordance with the physical prior, and improve the model's adaptability to complex environments and physiological regulatory mechanisms.

d. Performance Evaluation Metrics

To systematically compare the prediction performance of the physical baseline, XGBoost, and fusion residual model on different datasets, four metrics were used: root mean square error (RMSE), mean absolute error (MAE), mean absolute percentage error (MAPE), and coefficient of determination (R^2). Given a total of n samples, then

1. Root mean square error

$$\text{RMSE} = \sqrt{\frac{1}{n}\sum_{i=1}^{n}(E_i - \hat{E}_i)^2} \tag{10}$$

2. Mean absolute error

$$\text{MAE} = \frac{1}{n}\sum_{i=1}^{n}|E_i - \hat{E}_i| \tag{11}$$

3. Mean absolute percentage error

$$\text{MAPE} = \frac{100\%}{n}\sum_{i=1}^{n}\left|\frac{E_i - \hat{E}_i}{E_i}\right| \tag{12}$$

4. Coefficient of determination

$$R^2 = 1 - \frac{\sum_{i=1}^{n}(E_i - \hat{E}_i)^2}{\sum_{i=1}^{n}(E_i - \bar{E}_i)^2} \tag{13}$$

where E_i is the observed transpiration rate, $\hat{E}_i$ is the model predicted value, and $\bar{E}_i$ is the average value of the observed values.

To analyze the contribution of each feature to evaporation prediction in the fusion residual model from a mechanistic perspective, the SHAP method based on Shapley values is used to perform a posterior interpretation of the XGBoost residual model. SHAP decomposes the prediction of the complex model into the additive contributions of each input feature. For any sample i, the residual prediction $\hat{r}_i$ can be written as

$$\hat{r}_i = \phi_0 + \sum_{j=1}^{p}\phi_{ij} \tag{14}$$

where ϕ_0 is the expected baseline value of the model output on the training data, ϕ_{ij} is the marginal contribution of the j-th feature to the prediction of sample i, p is the total number of features, and for each j, its global importance can be measured by the average of the absolute values of its contributions across all samples

$$I_i = \frac{1}{n}\sum_{i=1}^{n}|\phi_{ij}| \tag{15}$$

C. Experimental Results and Analysis

The performance comparison of the models shows that the fusion model achieved the best performance in all indicators. Among them, MAE, RMSE, and MAPE all reached the lowest values among the three models, and R^2 also improved to 0.997, which almost completely matched the observed values, showing excellent prediction accuracy and stability. In order to fully demonstrate the effectiveness of the "physical prior + residual learning" strategy in the simulation of leaf transpiration and to ensure the fairness of the test, this paper uses the same dataset to verify the performance of the back propagation neural network (BPNN) [31], long short-term memory (LSTM) [32], and radial basis function (RBF) [33] models respectively. The results are shown in Table 2.

a. Relationship between Data Features and Key Variables

Trmmol is mainly concentrated in the range of 3–7 $\text{mmol}\cdot\text{m}^{-2}\cdot\text{s}^{-1}$, Photo is most concentrated around 5–15 $\mu\text{mol}\cdot\text{m}^{-2}\cdot\text{s}^{-1}$, Cond is mainly in the range of 0.2–0.6 $\text{mol}\cdot\text{m}^{-2}\cdot\text{s}^{-1}$, and VpdL is concentrated in the range of approximately 1.0–1.8 kPa. This indicates that the data cover a wide range of physiological states from low to high, with sufficient dynamic range, which is conducive to subsequent model

Table 2 Comparison of model results.

Model	MAE	RMSE	MAPE (%)	R^2
Physical	0.110	0.164	3.87	0.986
XGB	0.065	0.122	3.35	0.989
Phy-XGB	0.030	0.058	1.10	0.997
BPNN	0.075	0.115	3.12	0.990
LSTM	0.199	0.261	5.66	0.950
RBF	0.052	0.116	2.79	0.990

learning of the gradient response of transpiration to photosynthesis, stomatal conductance, and VPD, and is beneficial to improving the stability of model training. Therefore, Fig. 2 not only shows the range of variable values, but also proves that the dataset in this study has a good foundation in terms of representativeness and modelability.

The scatter plot further reveals the coupling characteristics of Trmmol with key driving factors. Trmmol shows a near-linear and close relationship with the physical prior E_{phys} = Cond × VpdL, indicating that $E \approx g_s \times$ VPD can well characterize the first-order physical trend of transpiration on this dataset. Trmmol also shows an overall positive correlation with Photo, but the point cloud distribution is significantly more discrete, reflecting that transpiration is not only limited by photosynthesis but also jointly controlled by factors such as VpdL and stomatal regulation. Transpiration is highest at moderate VpdL, while it is relatively lower under extremely low and high VpdL conditions, suggesting a certain degree of protective regulation of stomata at both the dry and wet ends, as shown in Fig. 3.

b. Model Performance Comparison

The fusion model performed best across all evaluation metrics. Compared to the physical baseline model, the fusion model reduced MAE and RMSE by approximately 72.7% and 64.6%, respectively, and MAPE by approximately 71.6%. Compared to the XGBoost model, the fusion model further reduced MAE and RMSE by approximately 53.8% and 52.4%, respectively, and MAPE by approximately 67.1%. Simultaneously, the R^2 increased to 0.997, significantly higher than the other two. This indicates that the fusion strategy, which incorporates physical priors and employs residual learning, significantly enhances the accuracy and stability of transpiration rate prediction, as shown in Fig. 4.

Beyond statistical metrics, the achieved accuracy is practically meaningful for irrigation decision support. The test RMSE of 0.0583 mmol·m^{-2}·s^{-1} is around the ~1% level relative to typical transpiration rates in our dataset (approximately 3–7 mmol·m^{-2}·s^{-1}), indicating highly reliable point-wise prediction. Converting this RMSE to an equivalent water-depth error yields ~0.023 mm over a 6 h observation window at the leaf scale (and ~0.07 mm after upscaling with LAI = 3), which is negligible compared with common daily

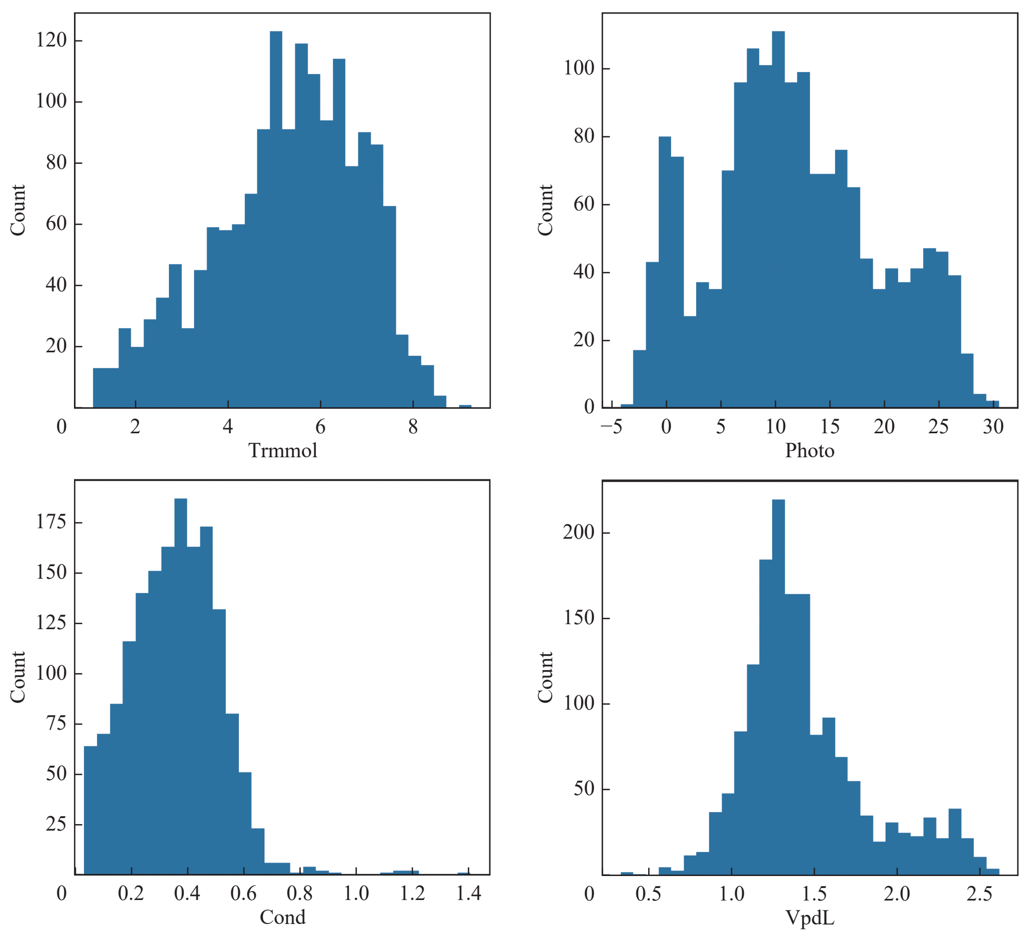

Fig. 2 Distributions of key variables.

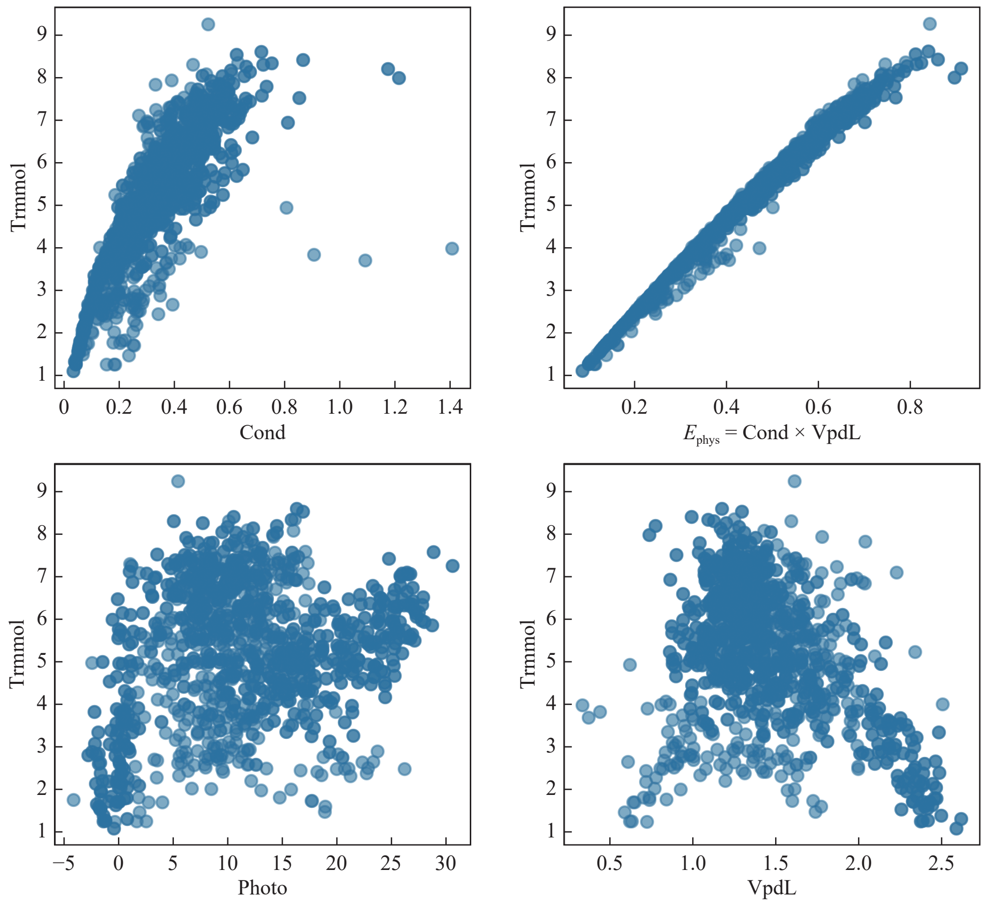

Fig. 3 Transpiration-driver relationships.

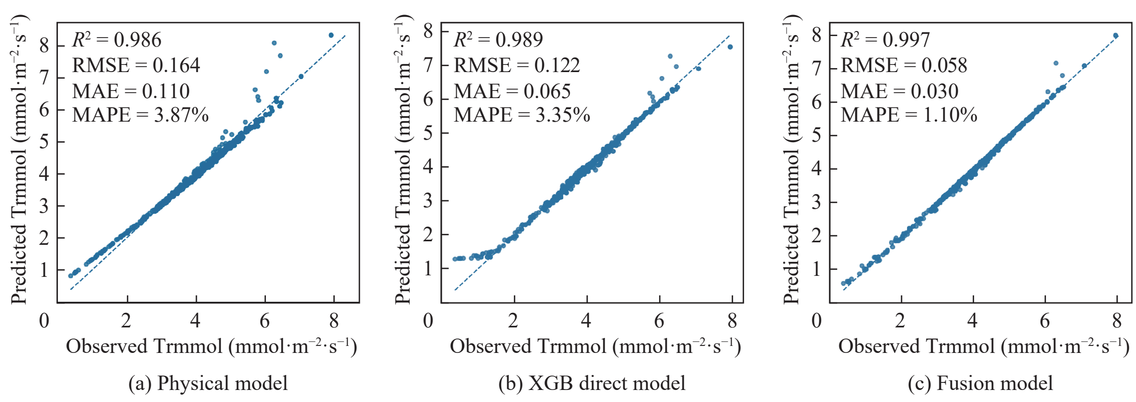

Fig. 4 Model prediction comparison.

irrigation depths (e.g., 6–26 mm·day^{-1} in our scenarios). This conversion assumes that 1 kg·m^{-2} water equals 1 mm water depth, integrates the flux over the 6 h window (Δt = 2.16 × 10^4 s), and upscales from leaf to canopy using $ET_{canopy} \approx ET_{leaf} \times$ LAI (LAI = 3). Therefore, the model accuracy is sufficient to support day-to-day irrigation scheduling and scenario comparison. Furthermore, the independent test result of $R^2 \approx 0.997$ indicates that the model can explain approximately 99.75% of the observed evapotranspiration variance, demonstrating its ability to faithfully reproduce the relative temporal fluctuations and condition-dependent responses under different greenhouse control schemes. Combined with a low RMSE, this confirms the accuracy of the trend and the precision of its magnitude, which is crucial for irrigation planning (e.g., identifying periods of high water demand and comparing different schemes).

The physical baseline exhibits a systematic underestimation in the high evaporation range, while the fusion model almost closely follows the 1:1 line across the entire gradient. This indicates that residual learning effectively corrects the weakest segment of the physical model, the high evaporation range, achieving a highly consistent fit in both magnitude and form. The residual-prediction scatter plot and residual histogram in the lower row show that the residuals of the fusion model are concentrated in a narrow range near zero, with no structural trend that changes with the predicted values. The error mainly manifests as small random fluctuations rather than systematic biases, as shown in Fig. 5.

The residual distributions of the physical model and the XGB model are relatively wide and slightly skewed, indicating that there are still some systematic biases and instabilities. In contrast, the residual distribution of the fusion model is the most concentrated and approximately symmetrical to zero, indicating that the errors are mainly small random fluctuations and the systematic biases have been effectively eliminated. This supports the advantages of the fusion model in robustness and physical consistency from a statistical distribution perspective, as shown in Fig. 6.

c. Feature Importance Analysis

E_{phys} was the dominant factor, indicating that stomatal conductance and leaf-air vapor pressure difference are key driving factors for transpiration rate prediction. VpdL and Cond followed closely, further validating the main influence of these physical factors on transpiration, as shown in Fig. 7.

d. Carbon-Water Trade-Off

The structure of the “leaf carbon gain-water cost” is visually presented through three relationships. The significant variation in transpiration at similar photosynthetic levels indicates that Photo alone cannot explain the differences in water consumption. A higher iWUE corresponds to a lower upper

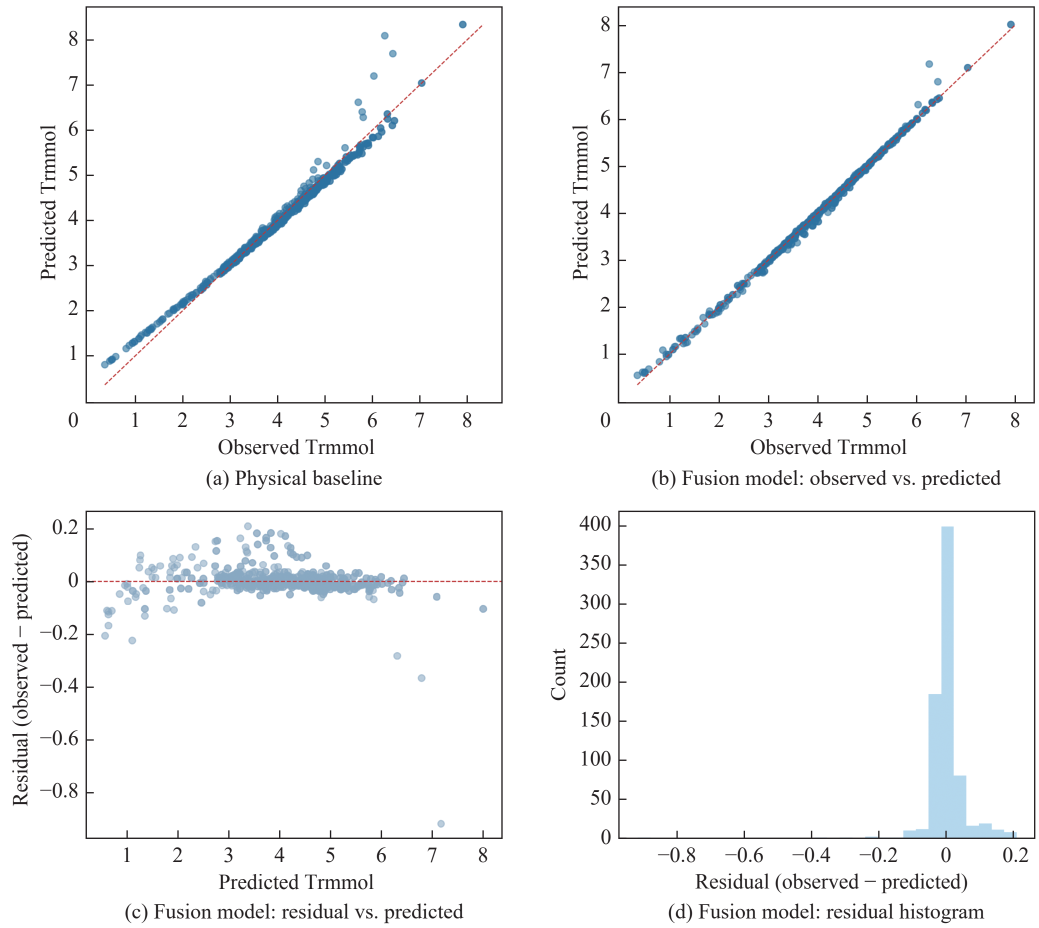

Fig. 5 Model residual patterns.

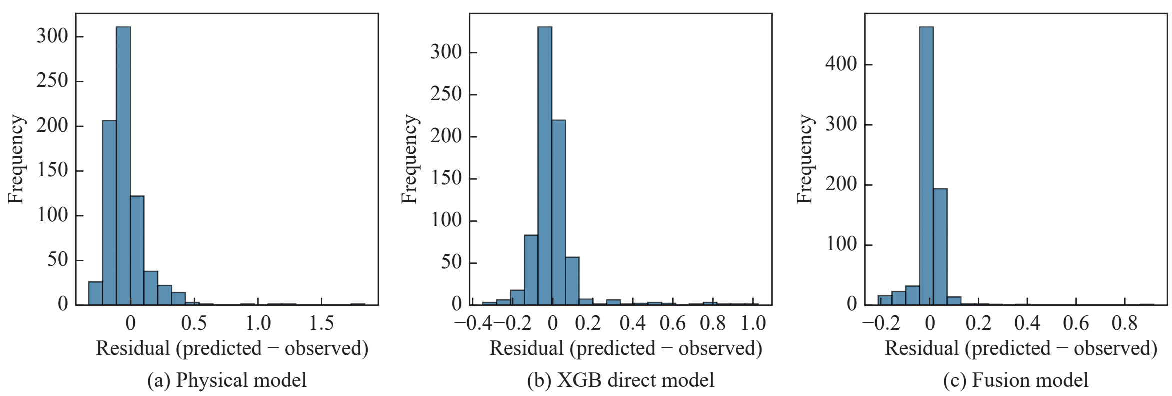

Fig. 6 Residual distributions of models.

limit for transpiration, clearly revealing the trade-off between water use efficiency and water consumption intensity. The extremely high and dispersed CTE values in the low photosynthetic zone indicate an uneconomical state of "high water consumption, low yield" during weak light or limited photosynthetic stages. This demonstrates that features such as E_{phys}, iWUE, and CTE capture different carbon-water strategies and transpiration cost patterns, providing a solid physiological basis for using these derived indicators in the fusion model, as shown in Fig. 8.

e. SHAP Interpretability Analysis

In the residual model, VpdL, E_{phys}, and Cond are the absolute dominant factors, contributing far more than other environmental and physiological variables. This indicates that the model primarily performs nonlinear corrections around the physical core composed of stomatal conductance and VPD. The SHAP curves of E_{phys} and VpdL both exhibit a saturation pattern of "increasing first and then slowing down", indicating that the model raises the physical baseline in the medium-to-high transpiration range and automatically applies an "upper limit" under extreme conditions. Cond's SHAP value turns significantly negative in the high conductance region, indicating that when stomata are strongly open, the residual model tends to lower the physical prediction, consistent with the theoretical expectation that transpiration tends to saturate and is hydraulically limited under high conductance. The color gradient also shows the interaction effect between Cond and VpdL and E_{phys}, as shown in Fig. 9.

Importantly, SHAP also reveals interaction-driven corrections rather than single-factor effects. When VpdL increases under moderate Cond, the model tends to add positive residuals, suggesting that the linear physics baseline underestimates transpiration in the medium-to-high demand regime. In contrast, under high VpdL accompanied by reduced Cond (stomatal regulation), residuals become negative, indicating an implicit "upper-limit" correction consistent with protective stomatal closure. Moreover, at very high Cond, SHAP values turn negative, implying saturation/hydraulic or energy constraints that prevent transpiration from increasing proportionally with g_s. These patterns highlight that the residual learner mainly acts as a regime-dependent modifier of the $g_s \times$ VPD physics.

f. Interaction Effects and Regime-Dependent Residual Correction

To further explore how factor interactions drive residual correction (beyond first-order physical processes), this paper calculates the SHAP interaction values of the XGBoost residual model and visualizes the joint response surface using a

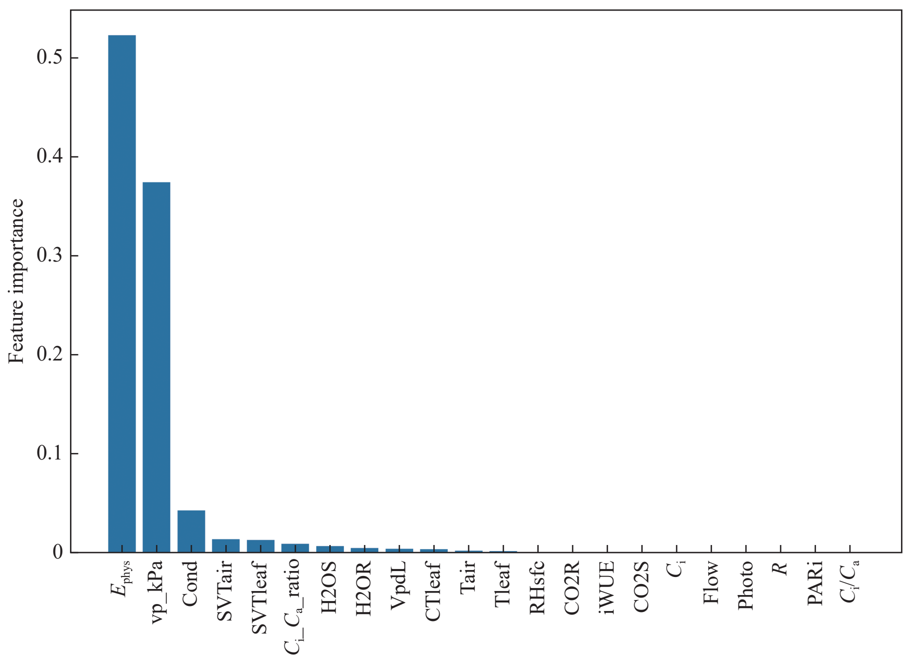

Fig. 7 Feature importance of XGBoost.

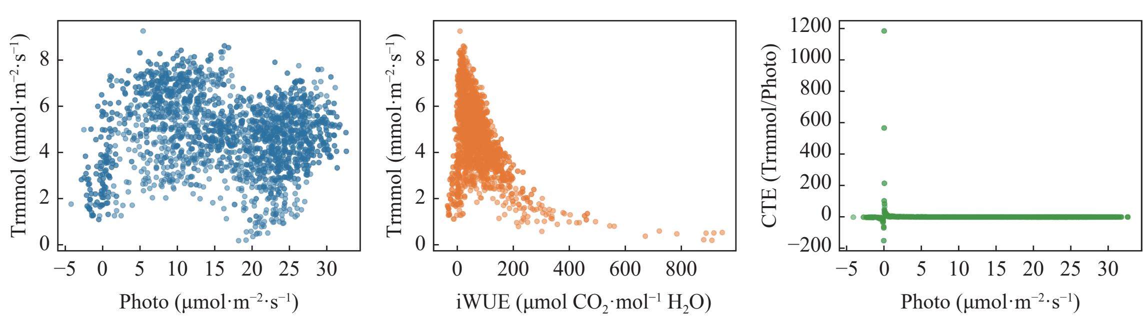

Fig. 8 Carbon-water relationship patterns.

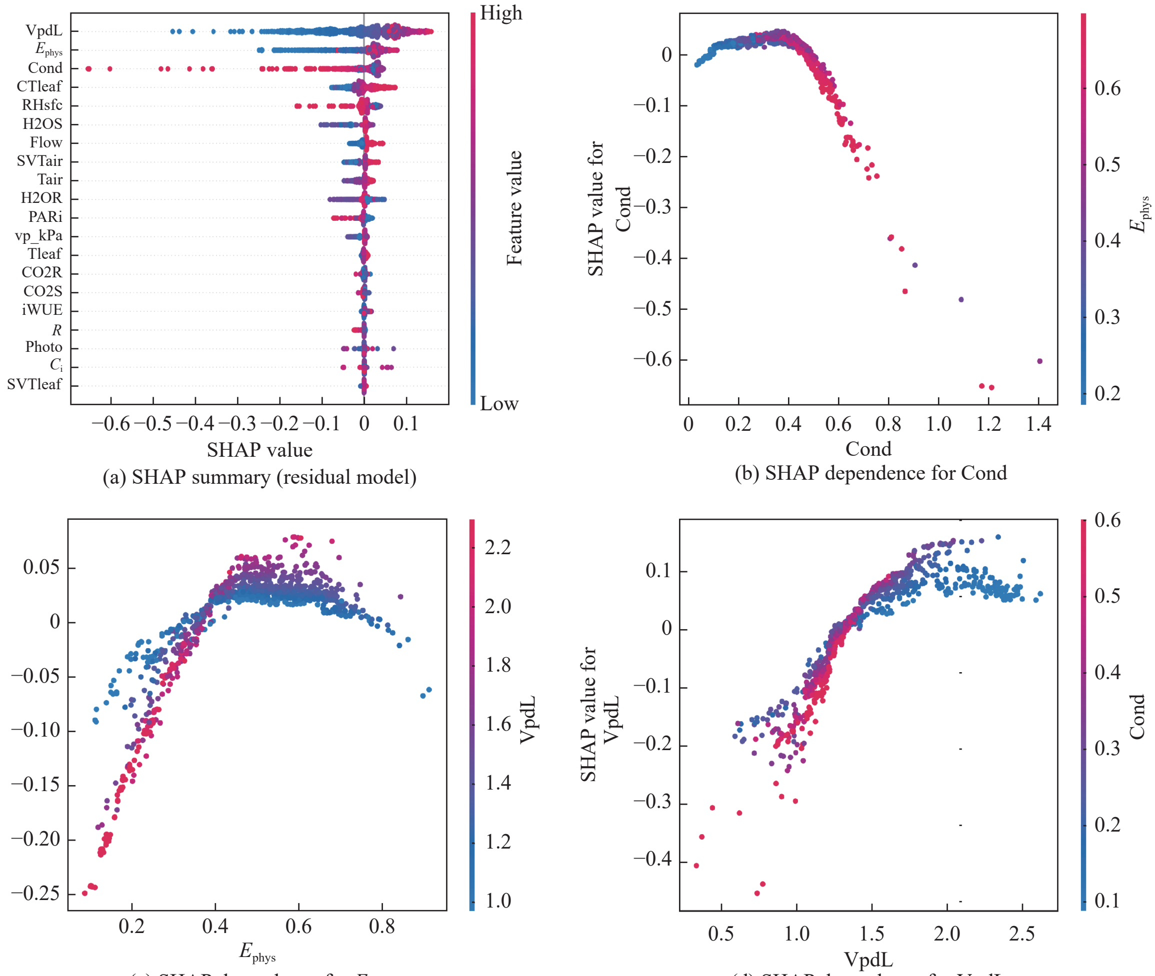

(a) SHAP summary (residual model)

(b) SHAP dependence for Cond

(c) SHAP dependence for E_{phys}

(d) SHAP dependence for VpdL

Fig. 9 SHAP dependence plots.

two-dimensional partial dependency plot (PDP), as shown in Figs. 10–12.

Fig. 10 shows the mean absolute SHAP interaction heatmap for the XGBoost residual model, which reflects the strength of pairwise interactions contributing to residual correction.

Fig. 11 presents the two-dimensional partial dependence of the residual output over the VpdL-Cond grid, illustrating the regime-dependent correction surface added to the physics-based baseline.

Fig. 12 shows the SHAP dependence plot for VpdL, colored by Cond, highlighting how the effect of atmospheric demand on residual correction is modulated by stomatal conductance.

E. Irrigation Decision Support

Building upon the preceding sections, the model predictions are scaled up to canopy evapotranspiration and daily irrigation demand. Two typical irrigation scenarios are constructed to compare the differences between empirical fixed irrigation strategies and model-based on-demand irrigation in terms of water use, energy consumption, and potential emission reductions. The aim is to answer the question of “how much water should be used and when should it be used”.

a. Model-Driven Estimation of Daily Irrigation Demand

The leaf transpiration rate derived from Trmmol fusion was first integrated over time, and its units were then converted to estimate the daily irrigation demand. Considering that the greenhouse tomato canopy structure is relatively uniform, and combined with actual measurements [34, 35], the leaf area index was taken to be 3, and the daily evapotranspiration at the canopy scale was obtained accordingly [36, 37].

$$\mathrm{ET}_{\mathrm{canopy,day}} = \mathrm{LAI} \times \mathrm{ET}_{\mathrm{leaf,day}} \tag{16}$$

$$\mathrm{Leafflux} \times \mathrm{Leafareaindex} = \mathrm{Canopyflux} \tag{17}$$

Within a simplified framework that does not consider changes in rainfall and soil water storage, this paper defines “on-demand irrigation” as matching irrigation depth with daily evapotranspiration [38, 39].

$$I_{\mathrm{model,day}} = \mathrm{ET}_{\mathrm{canopy,day}} \tag{18}$$

Full compensation irrigation is equivalent to compensating for the crop evapotranspiration of the day.

The resulting $I_{\mathrm{model,day}}$ inherits the high accuracy of the leaf-scale model and directly corresponds to the water budget at the canopy level, serving as an irrigation baseline for subsequent scenario comparisons.

b. Irrigation Scenario Setting

To reflect common but distinctly different management strategies in production, this paper sets up two empirical irri-

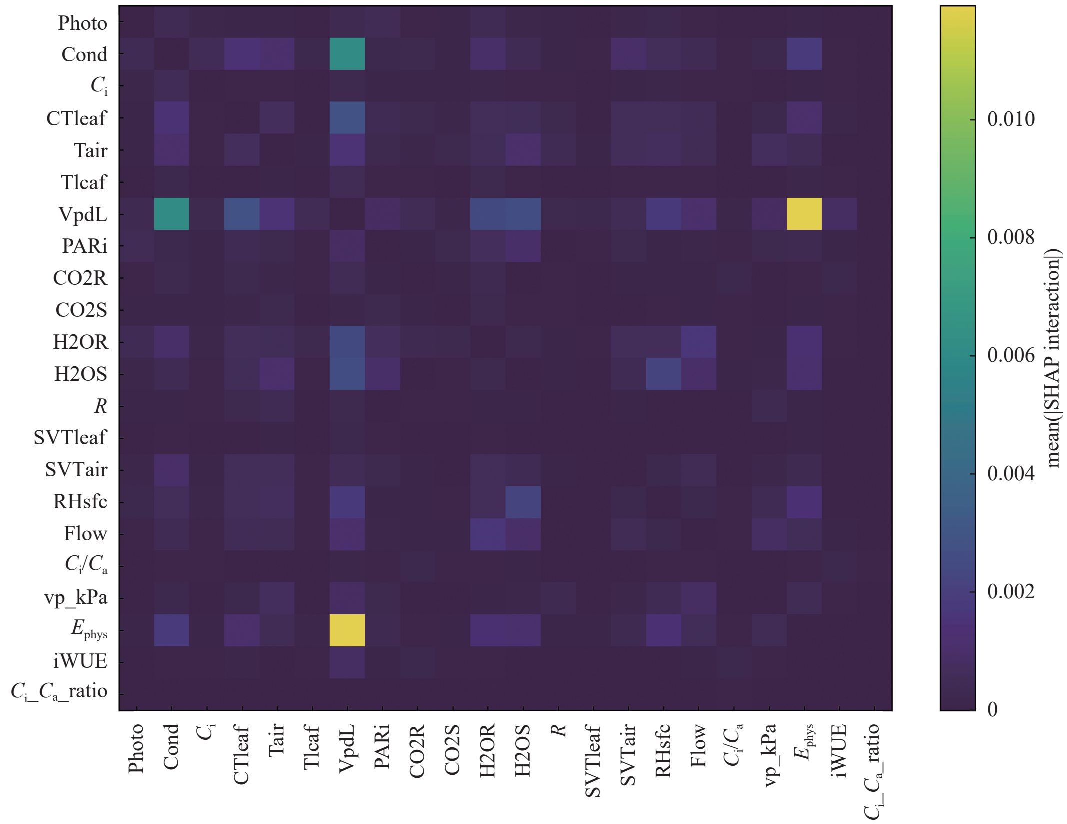

Fig. 10 Mean absolute SHAP interaction heatmap of XGBoost residual model.

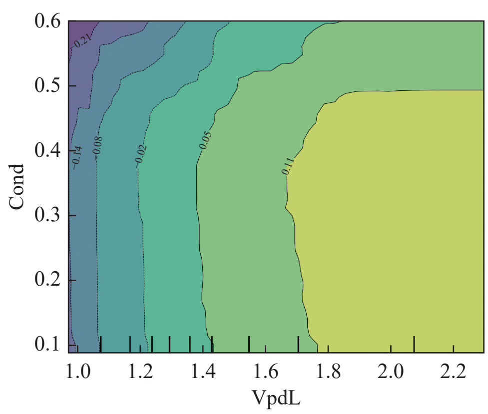

Fig. 11 Two-dimensional residual output diagram.

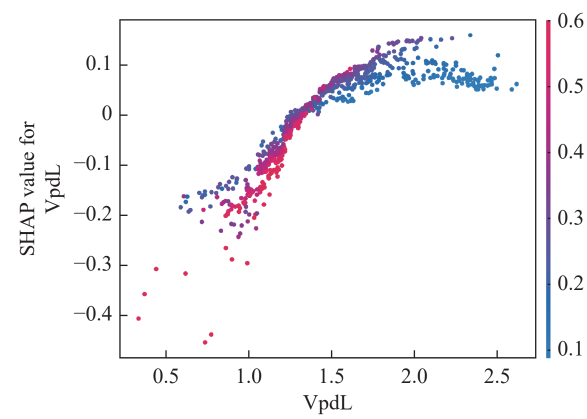

Fig. 12 SHAP dependency graph.

gation scenarios and compares them with the model's on-demand irrigation:

Scenario A: Fixed low-volume irrigation (under-irrigation baseline) Based on previous experience [40, 41], fixing the daily irrigation depth to 6 mm·day^{-1} represents a traditional approach aimed at "conservative water conservation". This scenario does not adjust the water volume according to weather and evapotranspiration changes, and is prone to cumulative deficits on days with high water demand.

Scenario B: Constant high-volume irrigation designed based on peak flow (over-irrigation baseline) Based on the ET peak predicted by the model during the study period, the daily irrigation depth is set to a constant close to the peak water demand (approximately 26 mm·day^{-1}). This represents a strategy of "upper limit irrigation" designed according to the most unfavorable conditions throughout the season, which can minimize water shortage, but may cause over-irrigation on most days with low to medium water demand.

Under the above scenario, the total irrigation depth during the study period is obtained by comparing the daily irrigation volume with the model's on-demand irrigation ($I_{\text{model,day}}$). Combining typical pumping energy consumption coefficients and electricity emission factors, excess or insufficient irrigation volume is converted into changes in pumping energy consumption per unit area and corresponding emission changes to quantify resource efficiency differences. For practical deployment, the proposed framework can be integrated into existing greenhouse fertigation systems by translating

$I_{\mathrm{model,day}}$ into irrigation duration/pulses under operational constraints (minimum/maximum daily depth and safety margins). VPD can be obtained from standard temperature-humidity sensors (and leaf temperature when available), while stomatal conductance can be estimated using parsimonious proxy models driven by radiation, CO_2, and VPD when direct measurements are unavailable. A closed-loop implementation can further combine the model with soil moisture/weight-based feedback to recalibrate parameters online and trigger alarms when persistent deviations occur, thereby improving robustness in real production.

c. Irrigation Results and Significance

A comparison of daily $\mathrm{ET}_{\mathrm{canopy,day}}$ and three irrigation schemes (scenario A, scenario B, and model-based on-demand irrigation) during the study period shows that on sunny days with high radiation and high VPD, the model-predicted daily evapotranspiration demand is much higher than 6 mm·day^{-1}, while it is close to or slightly lower than this value under cloudy or high humidity conditions, as shown in Fig. 13.

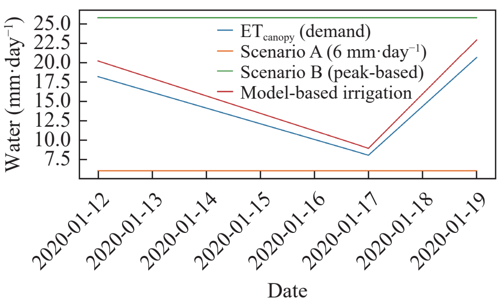

Fig. 13 Daily canopy ET and irrigation.

In terms of total volume, the total irrigation depth of scenario A during the experimental period was only about one-third of that of the model's on-demand irrigation, while that of scenario B was about 1.5 times that of the model's on-demand irrigation, as shown in Fig. 14.

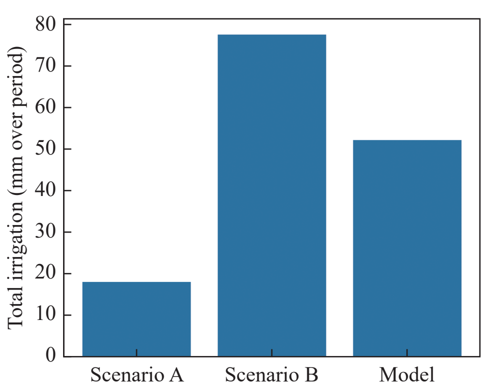

Fig. 14 Total irrigation by scenario.

Scenario A: Long-term mild to moderate under-irrigation In most high water demand weather conditions, a fixed irrigation amount of 6 mm·day^{-1} is far from sufficient to compensate for $\mathrm{ET}_{\mathrm{canopy,day}}$, leading to a continuous accumulation of net water deficit. Combined with SHAP analysis, high VPD and elevated leaf surface temperature are important driving factors for high transpiration days. The lack of corresponding irrigation response under scenario A easily leads to prolonged partial closure of stomata, limited photosynthesis, and potential yield loss.

Scenario B: Significant over-irrigation and resource waste For most days with low to medium water demand, the daily irrigation volume in scenario B is significantly higher than that in $\mathrm{ET}_{\mathrm{canopy}}$ and $I_{\mathrm{model,day}}$, only approaching the model scenario on a few peak water demand days. The total irrigation volume in scenario B is about one-third more than the model's on-demand irrigation, which translates to a similarly proportional increase in pumping energy consumption and CO_2 emissions. Since the excess water does not significantly improve photosynthetic levels and yield potential, scenario B effectively reduces water consumption efficiency and energy utilization efficiency per unit yield.

The trade-off advantages of model-based on-demand irrigation The model can provide irrigation amounts close to $\mathrm{ET}_{\mathrm{canopy}}$ on days with high water demand, significantly higher than in scenario A, thus reducing the risk of water stress. On days with low water demand, it automatically reduces irrigation amounts to avoid systematic over-irrigation as in scenario B. If scenario B is taken as the upper limit, the model's on-demand irrigation can save approximately 30% of irrigation water during the experimental period, and correspondingly reduce pumping energy consumption and indirect CO_2 emissions by the same amount, improving water and energy utilization efficiency while ensuring crop water supply.

d. Chapter Summary

This paper, for the first time, scales up a leaf-scale Physics + XGBoost model to irrigation scenario analysis, realizing a complete chain from mechanistic understanding to agricultural management. Two typical empirical irrigation strategies—under-irrigation (scenario A) and over-irrigation (scenario B)—were constructed and compared with model-driven on-demand irrigation. The results show that the fixed low-water-volume strategy generally carries a moderate risk of under-irrigation on days with high water demand, while the constant high-water-volume strategy designed based on peak demand results in significant over-irrigation on most days. Model-driven on-demand irrigation provides a compromise between the two, balancing disaster reduction and water conservation. In greenhouse tomato production, introducing a leaf-scale transpiration model not only improves the accuracy of evapotranspiration estimation but also helps identify blind spots in empirical irrigation regimes and provides a quantitative basis for developing irrigation strategies that balance yield and resource efficiency.

II. Conclusions

This paper constructs a unified dataset including derived indices E_{phys}, iWUE, CTE, and C_i/C_a. Data analysis shows that Trmmol is concentrated in the range of 3–7 mmol·m^{-2}·s^{-1}, and Photo, Cond, and VpdL cover a wide range of physiological states from low to high, providing a good foundation for modeling the gradient response of transpiration to photosynthesis, stomatal conductance, and water vapor pressure difference.

Based on this, this paper proposes a fusion modeling framework of "Physics + XGBoost residual learning". After introducing XGBoost residual learning, compared with the physical baseline, MAE and RMSE are reduced by about 72.7% and 64.6%, respectively, and MAPE is reduced by about 71.6%; compared with XGBoost, MAE and RMSE are further reduced by about 53.8% and 52.4%, respectively, and MAPE is reduced by about 67.1%.

Feature importance and SHAP interpretability analysis showed that VpdL, E_{phys}, and Cond were the key factors that dominated the correction of transpiration residuals, while derived indices such as iWUE and CTE revealed different carbon-water strategies from the perspectives of water use efficiency and transpiration cost per unit of photosynthetic yield, providing physiological support for understanding the behavior of the model at different environmental gradients.

Under LAI = 3, two irrigation scenarios were constructed, achieving a "scenario A + scenario B + model" approach that improved water and energy use efficiency while ensuring crop water supply, realizing a compromise optimization scheme of "controllable under-irrigation risk + significant suppression of over-irrigation".

This paper introduces physical priors at the leaf scale and combines them with residual learning to achieve quantitative transfer from leaf gas exchange observations to irrigation decision parameters. This demonstrates that the Physics + XGBoost + SHAP framework can serve as a general tool connecting physiological processes and irrigation management, and has the potential to be extended to other greenhouse crops and open fields in the future. Furthermore, it can be combined with crop models or regional evapotranspiration estimation to support multi-scale water management and clean agricultural production. From a theoretical perspective, the proposed physics-guided residual learning framework provides evidence that data-driven corrections can recover regime-dependent limitations (e.g., saturation and upper-bound behavior) beyond the first-order $g_s \times$ VPD relationship, aligning with stomatal regulation theory. This bridges mechanistic understanding and machine-learning flexibility and offers an interpretable pathway from leaf-level processes to actionable irrigation decision variables. Future work will also explore practical deployment when direct stomatal conductance measurements are unavailable.

Acknowledgment

We thank Associate Professor Miao Huang for support with data collection and for helpful discussions, and we acknowledge the public release of the dataset by Manjarrez-Sanchez and Martinez-Carrillo in 2020.

References

[1] M. Yao, M. Gao, J. Wang, B. Li, L. Mao, M. Zhao, Z. Xu, H. Niu, T. Wang, L. Sun et al., Estimating evapotranspiration of greenhouse tomato under different irrigation levels using a modified dual crop coefficient model in Northeast China, *Agriculture*, 2023, 13(9), 1741.

[2] R. Giuliani, N. Koteyeva, E. Voznesenskaya, M. A. Evans, A. B. Cousins, and G. E. Edwards, Coordination of leaf photosynthesis, transpiration, and structural traits in rice and wild relatives (genus *Oryza*), *Plant Physiol.*, 2013, 162(3), 1632–1651.

[3] M. Centritto, M. Lauteri, M. C. Monteverdi, and R. Serraj, Leaf gas exchange, carbon isotope discrimination, and grain yield in contrasting rice genotypes subjected to water deficits during the reproductive stage, *J. Exp. Bot.*, 2009, 60(8), 2325–2339.

[4] W. Ma, Y. Yu, X. Wang, and X. Gong, Estimation of intrinsic water-use efficiency from $\delta^{13}C$ signature of C_3 leaves: Assumptions and uncertainty, *Front. Plant Sci.*, 2023, 13, 1037972.

[5] P. Petrík, A. Petek-Petrik, M. Mukarram, B. Schuldt, and L. J. Lamarque, Leaf physiological and morphological constraints of water-use efficiency in C_3 plants, *AoB Plants*, 2023, 15(4), plad047.

[6] J. M. Mathias and R. B. Thomas, Global tree intrinsic water use efficiency is enhanced by increased atmospheric CO_2 and modulated by climate and plant functional types, *Proc. Natl. Acad. Sci. USA*, 2021, 118(7), e2014286118.

[7] J. Urban, M. W. Ingwers, M. A. McGuire, and R. O. Teskey, Increase in leaf temperature opens stomata and decouples net photosynthesis from stomatal conductance in *Pinus* taeda and *Populus deltoides x nigra*, *J. Exp. Bot.*, 2017, 68(7), 1757–1767.

[8] Y. Wang, J. S. Sperry, W. R. L. Anderegg, M. D. Venturas, and A. T. Trugman, A theoretical and empirical assessment of stomatal optimization modeling, *New Phytol.*, 2020, 227(2), 311–325.

[9] C. L. Kibler, A. T. Trugman, D. A. Roberts, C. J. Still, R. L. Scott, K. K. Caylor, J. C. Stella, and M. B. Singer, Evapotranspiration regulates leaf temperature and respiration in dryland vegetation, *Agric. For. Meteorol.*, 2023, 339, 109560.

[10] M. M. Qaderi, A. B. Martel, and S. L. Dixon, Environmental factors influence plant vascular system and water regulation, *Plants*, 2019, 8(3), 65.

[11] D. C. Plett, K. Ranathunge, V. J. Melino, N. Kuya, Y. Uga, and H. J. Kronzucker, The intersection of nitrogen nutrition and water use in plants: New paths toward improved crop productivity, *J. Exp. Bot.*, 2020, 71(15), 4452–4468.

[12] S. H. Kim and J. H. Lieth, A coupled model of photosynthesis, stomatal conductance and transpiration for a rose leaf (*Rosa hybrida* L.), *Ann. Bot.*, 2003, 91(7), 771–781.

[13] T. N. Buckley, Modeling stomatal conductance, *Plant Physiol.*, 2017, 174(2), 572–582.

[14] C. Grossiord, T. N. Buckley, L. A. Cernusak, K. A. Novick, B. Poulter, R. T. W. Siegwolf, J. S. Sperry, and N. G. McDowell, Plant responses to rising vapor pressure deficit, *New Phytol.*, 2020, 226(6), 1550–1566.

[15] W. Ouyang, P. C. Struik, X. Yin, and J. Yang, Stomatal conductance, mesophyll conductance, and transpiration efficiency in relation to leaf anatomy in rice and wheat genotypes under drought, *J. Exp. Bot.*, 2017, 68(18), 5191–5205.

[16] F. Villarreal-Guerrero, A. Pinedo-Alvarez, and J. Flores-Velázquez, Control of greenhouse-air energy and vapor pressure deficit with heating, variable fogging rates and variable vent configurations: Simulated effectiveness under varied outside climates, *Comput. Electron. Agric.*, 2020, 174, 105515.

[17] G. Nikolaou, D. Neocleous, N. Katsoulas, and C. Kittas, Effects of cooling systems on greenhouse microclimate and cucumber growth under Mediterranean climatic conditions, *Agronomy*, 2019, 9(6), 300.

[18] M. Palumbo, M. D'Imperio, V. Tucci, M. Cefola, B. Pace, P. Santamaria, A. Parente, and F. F. Montesano, Sensor-based irrigation reduces water consumption without compromising yield and postharvest quality of soilless green bean, *Agronomy*, 2021, 11(12), 2485.

[19] Z. Wei, T. Du, X. Li, L. Fang, and F. Liu, Simulation of stomatal conductance and water use efficiency of tomato leaves exposed to different irrigation regimes and air CO_2 concentrations by a modified "Ball-Berry" model, *Front. Plant Sci.*, 2018, 9, 445.

[20] J. Manjarrez-Sanchez and G. Martinez-Carrillo, Dataset of photosynthesis and photosynthetic factors measurements of greenhouse tomato, *Data Brief*, 2020, 32, 106274.

[21] M. Niazkar, A. Menapace, B. Brentan, R. Piraei, D. Jimenez, P. Dhawan, and M. Righetti, Applications of XGBoost in water resources engineering: A systematic literature review (Dec 2018–May 2023), *Environ. Modell. Software*, 2024, 174, 105971.

[22] J. Ge, L. Zhao, Z. Yu, H. Liu, L. Zhang, X. Gong, and H. Sun, Prediction of greenhouse tomato crop evapotranspiration using XGBoost machine learning model, *Plants*, 2022, 11(15), 1923.

[23] U. Tunalı, I. H. Tüzel, Y. Tüzel, and Y. Şenol, Estimation of actual crop evapotranspiration using artificial neural networks in tomato grown in closed soilless culture system, *Agric. Water Manage.*, 2023, 284, 108331.

[24] S. Amani and H. Shafizadeh-Moghadam, A review of machine learning models and influential factors for estimating evapotranspiration using remote sensing and ground-based data, *Agric. Water Manage*., 2023, 284, 108324.

[25] X. Hu, L. Shi, G. Lin, and L. Lin, Comparison of physical-based, data-driven and hybrid modeling approaches for evapotranspiration estimation, *J. Hydrol.*, 2021, 601, 126592.

[26] H. Chen, J. Huang, S. S. Dash, Y. Wei, and H. Li, A hybrid deep learning framework with physical process description for simulation of evapotranspiration, *J. Hydrol.*, 2022, 606, 127422.

[27] X. Li, F. Xue, J. Ding, T. Xu, L. Song, Z. Pang, J. Wang, Z. Xu, Y. Ma, Z. Lu et al., A hybrid model coupling physical constraints and machine learning to estimate daily evapotranspiration in the Heihe River Basin, *Remote Sens*., 2024, 16(12), 2143.

[28] S. M. Lundberg and S. I. Lee, A unified approach to interpreting model predictions, in *Proc. 31st International Conference on Neural Information Processing Systems*, Long Beach, CA, USA, 2017, 4768–4777.

[29] J. Liang, K. W. Krauss, J. Finnigan, H. Stuart-Williams, G. D. Farquhar, and M. C. Ball, Linking water use efficiency with water use strategy from leaves to communities, *New Phytol.*, 2023, 240(5), 1735–1742.

[30] K. A. Simonin, E. Burns, B. Choat, M. M. Barbour, T. E. Dawson, and P. J. Franks, Increasing leaf hydraulic conductance with transpiration rate minimizes the water potential drawdown from stem to leaf, *J. Exp. Bot.*, 2015, 66(5), 1303–1315.

[31] J. Hu, P. Xin, S. Zhang, H. Zhang, and D. He, Model for tomato photosynthetic rate based on neural network with genetic algorithm, *Int. J. Agric. Biol. Eng.*, 2019, 12(1), 179–185.

[32] Y. Fan, W. Zhang, W. Zhang, D. Zhang, and L. He, A double-layer LSTM model based on driving style and adaptive grid for intention-trajectory prediction, *Sensors*, 2025, 25(7), 2059.

[33] L. Li, S. Chen, C. Yang, F. Meng, and N. Sigrimis, Prediction of plant transpiration from environmental parameters and relative leaf area index using the random forest regression algorithm, *J. Cleaner Prod.*, 2020, 261, 121136.

[34] E. Heuvelink, M. J. Bakker, A. Elings, R. C. Kaarsemaker, and L. F. M. Marcelis, Effect of leaf area on tomato yield, in *Proc. International Conference on Sustainable Greenhouse Systems-Greensys2004*, Leuven, Belgium, 2004, 43–50.

[35] S. A. A. M. Hossain, L. Wang, T. Chen, and Z. Li, Leaf area index assessment for tomato and cucumber growing period under different water treatments, *Plant Soil Environ.*, 2017, 63(10), 461–467.

[36] T. W. Gara, A. K. Skidmore, R. Darvishzadeh, and T. Wang, Leaf to canopy upscaling approach affects the estimation of canopy traits, *GISci. Remote Sens.*, 2019, 56(4), 554–575.

[37] M. S. Alam, D. W. Lamb, and N. W. M. Warwick, A canopy transpiration model based on scaling up stomatal conductance and radiation interception as affected by leaf area index, *Water*, 2021, 13(3), 252.

[38] B. R. Hanson and D. M. May, New crop coefficients developed for high-yield processing tomatoes, *Calif. Agric.*, 2006, 60(2), 95–99.

[39] S. Locatelli, W. Jr. Barrera, L. Verdi, C. Nicoletto, A. Dalla Marta, and C. Maucieri, Modelling the response of tomato on deficit irrigation under greenhouse conditions, *Sci. Hortic.*, 2024, 326, 112770.

[40] Harmanto, V. M. Salokhe, M. S. Babel, and H. J. Tantau, Water requirement of drip irrigated tomatoes grown in greenhouse in tropical environment, *Agric. Water Manage.*, 2005, 71(3), 225–242.

[41] M. Hong, Z. Zhang, Q. Fu, and Y. Liu, Water requirement of solar greenhouse tomatoes with drip irrigation under mulch in the Southwest of the Taklimakan Desert, *Water*, 2022, 14(19), 3050.

Guoqing Zhang received the BS degree from Tianjin Sino-German University of Applied Sciences, China, in 2024. He is currently pursuing the MS degree at School of Intelligent Manufacturing and Control Engineering, Shanghai Polytechnic University, Shanghai, China. His research interests include agricultural engineering and the coordinated optimization of crop yield with photosynthetic and transpiration rates.

Miao Huang received the PhD degree from East China University of Science and Technology, China, in 2015. She is currently an associate professor at School of Intelligent Manufacturing and Control Engineering, Shanghai Polytechnic University, China. Her research interests include smart agriculture, deep learning, and the theory and applications of control for complex nonlinear systems.

Lili Tao received the PhD degree from East China University of Science and Technology, China, in 2011. She is currently an associate professor at School of Intelligent Manufacturing and Control Engineering, Shanghai Polytechnic University, China. Her research interests include modeling and optimization of complex industrial processes.

Shuping Zhang received the PhD degree from Donghua University, China, in 2011. She is currently a lecturer at School of Intelligent Medicine and Health Engineering, Shanghai Polytechnic University, China. Her research interests include real-time modeling and adaptive optimal control of complex dynamic systems.